Influence of strain on the indium incorporation in (0001) GaN

T. Schulz,[1,*] L. Lymperakis,[2,†] M. Anikeeva,[1] M. Siekacz,[3] P. Wolny,[3] T. Markurt,[1] and M. Albrecht[1]

[1]*Leibniz-Institut für Kristallzüchtung, Max-Born-Str. 2, 12489 Berlin, Germany*

[2]*Max-Planck-Institut für Eisenforschung GmbH, Max-Planck-Str. 1, 40237 Düsseldorf, Germany*

[3]*Institute of High Pressure Physics, Polish Academy of Sciences, Sokolowska 29/37, 01–142 Warsaw, Poland*

(Received 4 March 2020; accepted 6 July 2020; published 24 July 2020)

The incorporation of indium in GaN (0001) surfaces in dependence of strain is investigated by combining molecular-beam epitaxy (MBE) growth, quantitative transmission electron microscopy, and density-functional theory (DFT) calculations. Growth experiments were conducted on GaN, as well as on 30% ± 2% partially relaxed $In_{0.19}Ga_{0.81}N$ buffer layers, serving as substrates. Despite the only 0.6% larger in-plane lattice constant of GaN provided by the buffer layer, our experiments reveal that the In incorporation increases by more than a factor of two for growth on the $In_{0.19}Ga_{0.81}N$ buffer, as compared to growth on GaN. DFT calculations reveal that the decreasing chemical potential due to the reduced lattice mismatch stabilizes the In–N bond at the surface. Depending on the growth conditions (metal rich or N rich), this promotes the incorporation of higher In contents into a coherently strained layer. Nevertheless, the effect of strain is highly nonlinear. As a consequence of the different surface reconstructions, growth on relaxed $In_xGa_{1-x}N$ buffers appears more suitable for metal-rich MBE growth conditions with regard to achieving higher In compositions.

DOI: 10.1103/PhysRevMaterials.4.073404

I. INTRODUCTION

Alloying InN and GaN in coherently grown quantum wells (QWs) offers the opportunity to cover the entire visible spectrum of light-emitting devices without the need of phosphors for conversion. Particularly for all red-green-blue micro-light-emitting diodes, the monolithic integration of a single material system is a desirable goal. Unfortunately, realizing longer emission wavelengths is hampered by a fundamental limitation in coherently grown layers for In compositions exceeding approximately 30%. Compositions in this range were quantified by atom probe tomography and transmission electron microscopy (TEM) [1,2]. Reports claiming substantially higher In compositions in coherently grown layers on GaN did not present detailed studies of the chemical composition, e.g., Ref. [3]. The limitation of the In incorporation is caused by a twofold dilemma: First, the necessity of progressively lower growth temperatures (and increasing N fluxes) due to the huge differences in the formation enthalpies between GaN and InN [4,5] may drive relaxed $In_xGa_{1-x}N$ into the miscibility gap [6,7]. Second, although compressive strain in coherently grown InGaN QWs may suppress phase separation [8–10], it promotes In segregation towards the surface—thus limiting In incorporation [11,12]. Compressive strain inhibiting In incorporation has been discussed in a number of early works, partly under the term of compositional pulling (e.g., Refs. [13–17]). Most of these studies observed an increased In incorporation upon plastic relaxation of the growing $In_xGa_{1-x}N$ film. More recent studies reveal that growth of $In_xGa_{1-x}N$ QWs on relaxed $In_xGa_{1-x}N$ buffers causes a redshift of the emission as compared to their counterparts on GaN, indicating an increased In content [18,19]. Thus, while qualitatively the effectiveness of the approach is evident, a quantitative analysis of the full potential of the approach and its possible limitations have not been explored yet.

In this paper, we combine density-functional theory (DFT) calculations with molecular-beam epitaxy (MBE) growth experiments and TEM studies to quantify the influence of strain on the incorporation of In into GaN. To avoid a complex strain state of the layer due to, e.g., a transition of the growth mode, we expose an unstrained and tensile-strained GaN (0001) surface to In an N flux only. This results in a substitution of Ga by In in the topmost III–V monolayer (ML) [20], which is finally capped by GaN thus representing a less complex model system. Tensile-strained GaN was realized via depositing a partially relaxed $In_xGa_{1-x}N$ film, grown on a GaN substrate. We show that QW growth on 0.6% tensile-strained GaN results in a more than two times higher In content as compared to growth on relaxed GaN, in quantitative agreement with DFT calculations. The driving force is a strong reduction of the indium chemical potential at the surface, even for small amounts of tensile strain. The benefit is twofold: The incorporation of indium at the surface is promoted for a given In flux while at the same time the stability of the In–N bond is increased, which reduces thermal decomposition. The relevance of these two factors strongly depends on the respective growth conditions, i.e., metal- or N rich. The twofold benefit makes this approach generally promising for expanding the growth window of high In content $In_xGa_{1-x}N$ QWs.

II. EXPERIMENT

Growth experiments were conducted by plasma-assisted molecular beam epitaxy using a Riber-VG90 system on

*tobias.schulz@ikz-berlin.de

†l.lymperakis@mpie.de

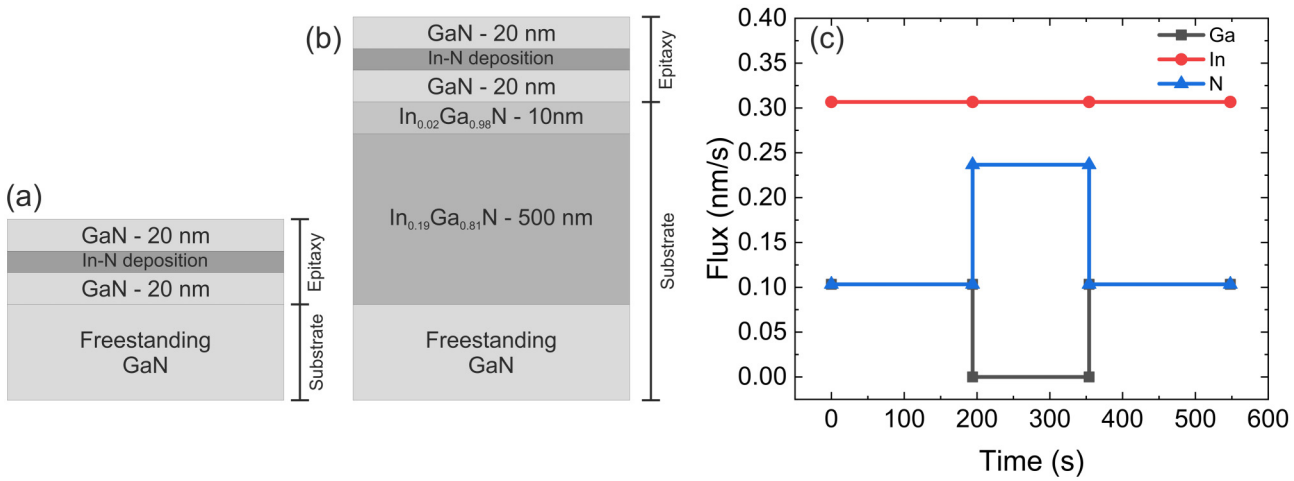

FIG. 1. (a), (b) Sketches of the two samples investigated in this study. (c) The In, Ga, and N fluxes during the epitaxy process.

freestanding GaN, as well as on a partially relaxed InGaN buffer layer, serving as a substrate. The freestanding GaN exhibits a threading dislocation density on the order of 10^7 cm^{-2} and a miscut angle of $\alpha = 0.65^\circ$ towards the $\langle 1\bar{1}00 \rangle$ direction. The InGaN buffer structure consists of freestanding GaN, which was overgrown by a 500-nm-thick, partially relaxed $In_{0.19}Ga_{0.81}N$ buffer and a pseudeomorphic 10-nm $In_{0.02}Ga_{0.98}N$ cap layer. The threading dislocation density of these substrates increases to 10^9 cm^{-2}. As confirmed by x-ray diffraction, the $In_{0.19}Ga_{0.81}N$ buffer layer is partially relaxed by $30\% \pm 2\%$, which provides a 0.6% larger in-plane lattice constant as compared to the freestanding GaN substrate. See Supplemental Material [21] for a reciprocal-space map of the $In_{0.19}Ga_{0.81}N$ buffer substrate. General information about the buffer growth and their characteristics can be found elsewhere [22].

The MBE growth experiments were carried out on the above-described two types of substrates. For the sake of comparability, both were coloaded, i.e., glued on a 2-in. GaN/sapphire template. The deposition temperature was fixed to 650 °C during the entire process under metal-rich conditions. First, a GaN barrier of 20 nm was deposited using a Ga flux of $\Phi_{Ga} = 0.10$ nm/s and a N flux of $\Phi_N = 0.10$ nm/s with an In flux of $\Phi_{In} = 0.31$ nm/s, with the latter serving under these conditions as a surfactant. Subsequently, for the InGaN QW deposition the Ga shutter was closed while the N flux was increased to $\Phi_N = 0.24$ nm/s for a duration of 160 s, while keeping the In flux constant. Finally, the QW was capped by a 20-nm GaN layer using the same fluxes as for the previous GaN layer. A sketch of the two structures, as well as the timeline of the MBE growth run, is displayed in Figs. 1(a), 1(b), and 1(c), respectively.

Structural and compositional analyses were performed by means of scanning transmission electron microscopy–high-angle annular dark field (STEM-HAADF) and TEM, respectively. Investigations were performed in an FEI Titan 80–300 operated at 300 kV. Cross-sectional samples were prepared in the $\langle 1\bar{1}00 \rangle$ and the $\langle 11\bar{2}0 \rangle$ axis by mechanical polishing and subsequent Ar^+ ion milling until electron transparency. Lattice parameter measurements were carried out using the approach described in Ref. [23]. STEM-HAADF was performed using an acceptance semiangle of 35 mrad of the annular dark-field detector with a convergence semiangle of 9 mrad. For TEM and STEM-HAADF image simulations, we used supercells consisting of a single $In_xGa_{1-x}N$ ML with Ga atoms being randomly substituted by In. The relaxation of the supercell was done using a ternary interatomic potential with periodic boundary conditions along all directions [24]. For the TEM image simulations we used an in-house software package, based on a standard multislice algorithm [25]. Weak phase functions were calculated with the EMS software package [26]. STEM multislice simulations were performed in accordance with the experimental conditions [27]. Low-temperature (4 K) photoluminescence (PL) experiments were carried out using the 325-nm line of a He-Cd laser for excitation. DFT calculations were performed within the local-density approximation. The surfaces were modeled with a slab geometry of 8-ML thickness and $(2\sqrt{3} \times 2\sqrt{3})R30^\circ$ surface unit cell. Further details on the calculations can be found elsewhere [11,20].

III. RESULTS AND DISCUSSION

Atomic force microscopy (AFM) images of the surfaces of both samples after epitaxy are displayed in Figs. 2(a) and 2(b), respectively. Although the InGaN buffer sample exhibits hillocks as a result of spiral growth due to the formation of $(a+c)$ misfit during plastic relaxation of the buffer, both surfaces show comparable monoatomic steps with terrace widths of around 20 nm corresponding to the initial miscut angle of the substrate. Thus, for both cases (0001) GaN terraces of comparable area were exposed to In and N making the QW growth conditions comparable.

Figures 3(a) and 3(b) show STEM-HAADF images of the QW region in the $\langle 11\bar{2}0 \rangle$ projection for the GaN and for the $In_{0.19}Ga_{0.81}N$ buffer sample, respectively. For all TEM studies we have deliberately chosen areas where a flat (0001) plane was exposed to In and N making the single monolayer thick InGaN QW observable without any steps. In both cases, the thickness of the QW is limited to a single ML, confirming

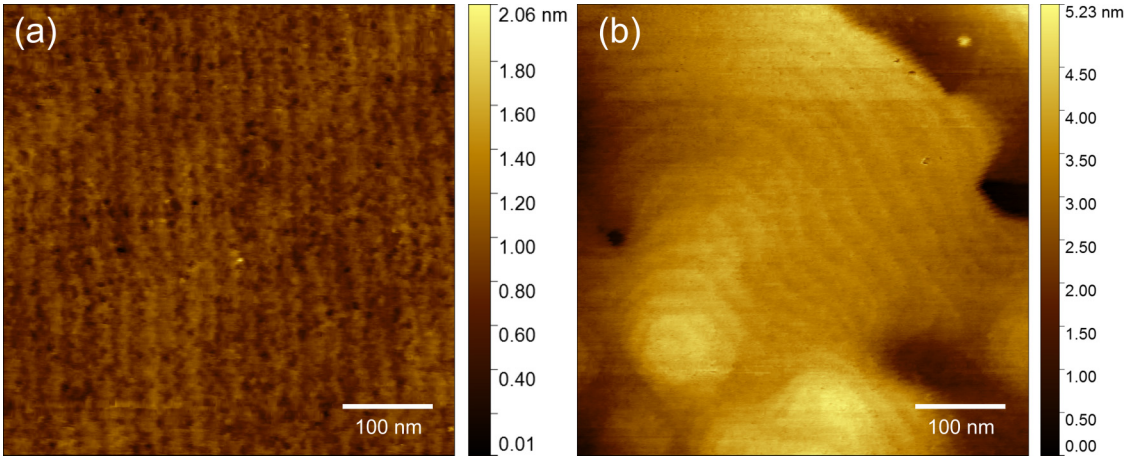

FIG. 2. AFM of the as-grown surfaces of the samples grown on the (a) GaN substrate and (b) $In_{0.19}Ga_{0.81}N$ buffer.

the self-limitation mechanism [20]. Laterally averaging the STEM-HAADF images in Figs. 3(a) and 3(b) with the signal recorded in the GaN region normalized to unity yields the profiles shown in Figs. 3(c) and 3(d), respectively. Apparently, the QW grown on the $In_{0.19}Ga_{0.81}N$ buffer appears at a much higher contrast with respect to the surrounding GaN, indicating an increased In content. The mean contrast in the QW region [indicated by the horizontal bars in Fig. 3(c) and 3(d)] reveals a ratio of around 1.04 for the GaN substrate and 1.12 for the $In_{0.19}Ga_{0.81}N$ buffer sample, respectively. To quantify the In composition of the MLs from these values, we carried out STEM-HAADF image simulations using a relaxed supercell consisting of a single $In_{0.25}Ga_{0.75}N$ monolayer. See Supplemental Material [21] for the STEM-HAADF contrast simulation of an $In_{0.25}Ga_{0.75}N$ monolayer with In atoms randomly distributed.

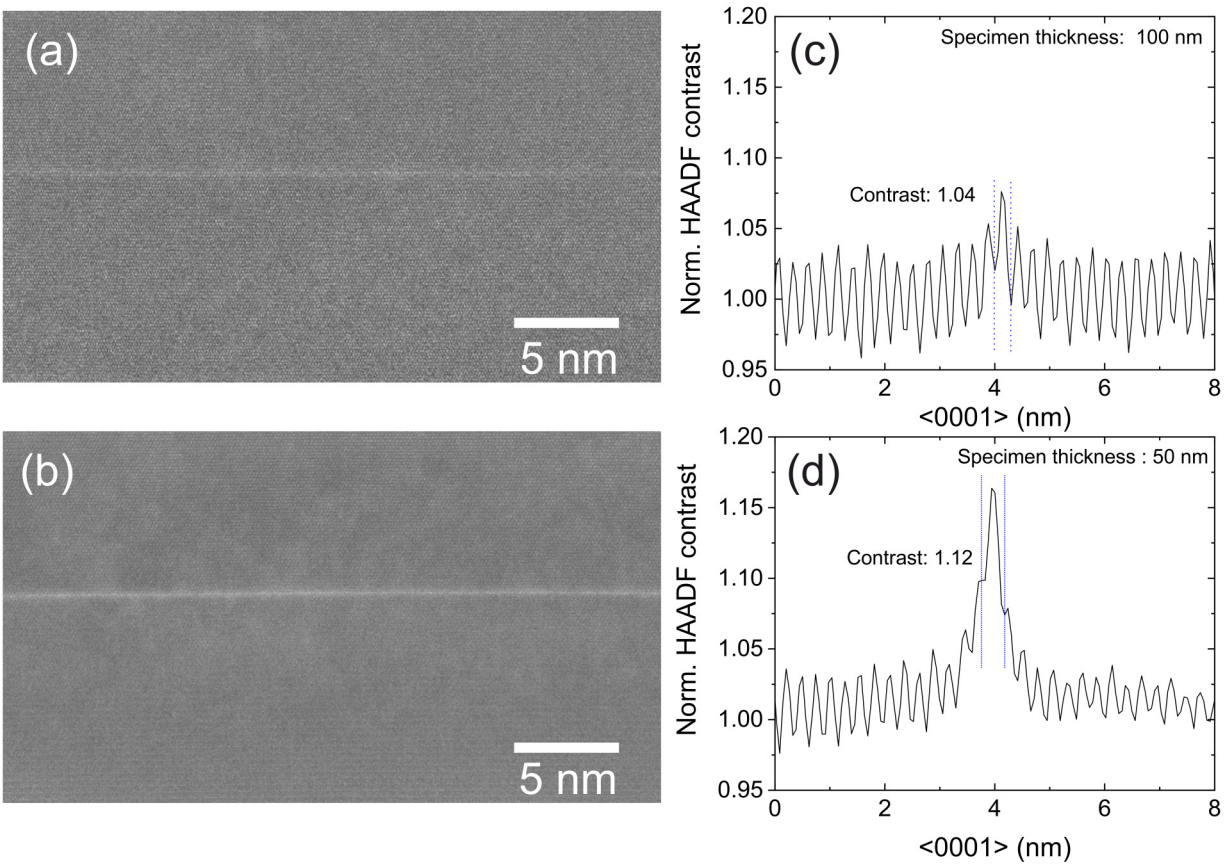

FIG. 3. STEM-HAADF images recorded in the $\langle 11\bar{2}0\rangle$ projection showing the nominal $In_xGa_{1-x}N$ QW region of the sample grown on (a) the GaN substrate and (b) the $In_{0.19}Ga_{0.81}N$ buffer. (c), (d) Horizontally averaged intensities of STEM-HAADF images (a) and (b), respectively. The vertical dashed lines enclose the QW region.

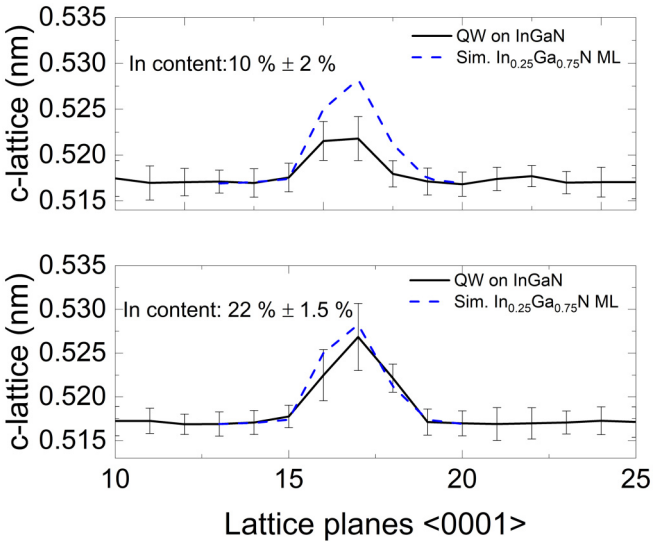

FIG. 4. Laterally averaged lattice parameter maps obtained from TEM images in the region of the $In_xGa_{1-x}N$ QWs grown on the (a) GaN and (b) $In_{0.19}Ga_{0.81}N$ buffer. Additionally, (a) and (b) show laterally averaged lattice maps obtained from image simulations of supercells consisting of a single ML thick $In_{0.25}Ga_{0.75}N$ QW (dashed line).

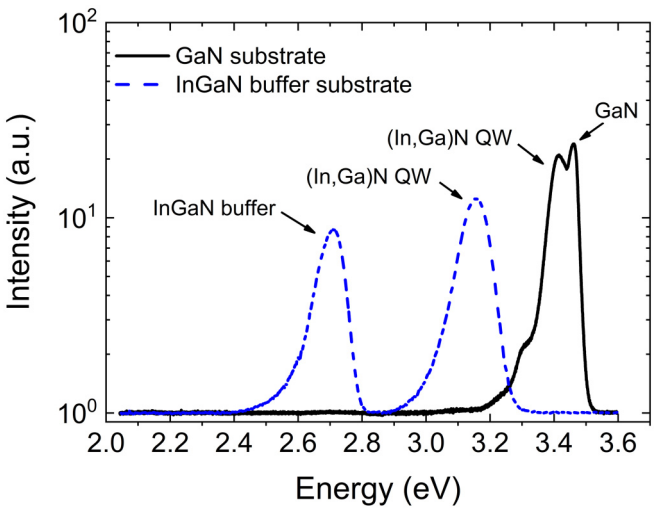

FIG. 5. PL measurements of $In_xGa_{1-x}N$ MLs grown on a GaN substrate (solid line) and on an $In_{0.19}Ga_{0.81}N$ buffer (dashed line) at 4 K.

Comparing the HAADF intensity in the GaN region, referenced to our detector sensitivity, allows us to determine sample thicknesses of 100 nm for the ML grown on GaN and 50 nm for the ML on the $In_{0.19}Ga_{0.81}N$ buffer, respectively. For these thicknesses, a single InGaN ML with an In content of 25% results in a mean contrast to GaN of 1.15 and 1.13, respectively. By a simple linear interpolation, we estimate In compositions of 8% for the ML on the GaN and 20% for the ML on the $In_{0.19}Ga_{0.81}N$ buffer, respectively. Complementary composition quantifications were carried out by TEM imaging. Subsequent mapping of the *c*-lattice parameters in the region of the $In_xGa_{1-x}N$ QW yields Figs. 4(a) and 4(b) for the sample grown on GaN and on the InGaN buffer, respectively. See Supplemental Material [21] for the respective TEM images. In this plot, the measured *c*-lattice parameters were averaged laterally over around 120 in-plane lattice planes, i.e., approximately 20 nm. The *c*-lattice parameters measured in the GaN barriers were normalized to $c_{GaN} = 0.517$ nm, which corresponds to the *c*-lattice parameter of GaN according to the utilized interatomic empirical potential [24]. In addition, Figs. 4(a) and 4(b) also show the measured lattice parameters in an image simulation of a supercell consisting of a single ML thick $In_{0.25}Ga_{0.75}N$ QW (dashed line). By linear interpolation between measured values in our samples and the value obtained for a simulated $In_{0.25}Ga_{0.75}N$ QW, we quantify $x = 0.1$ and $x = 0.22$ for growth on GaN substrate and the $In_{0.19}Ga_{0.81}N$ buffer, respectively.

Hence, our TEM investigations corroborate the trend found in the STEM-HAADF studies, confirming a more than two times higher In content in the QW grown on the partially relaxed $In_{0.19}Ga_{0.81}N$ buffer, as compared to the counterpart grown on GaN. Finally, we performed low-temperature PL experiments to investigate the compositional differences of the QWs on a more macroscopic scale, as shown in Fig. 5. For the sample grown on GaN we observe a peak very close to the emission of GaN, occurring at about 3.41 eV, which is typically observed for samples grown under comparable conditions. The emission of the QW on the $In_{0.19}Ga_{0.81}N$ buffer is substantially redshifted and located around 3.16 eV (393 nm) accompanied by a notable increase of the half-width of the band. Since the thickness of both QWs is limited to a single monolayer [20] where polarization fields have a negligible influence on the emission energy [28], this allows us to qualitatively conclude on the In content: Based on that, both the redshift of the emission, as well as the increased half-width of the emission band due to inhomogeneous broadening, support a higher In composition of the QW grown on the $In_{0.19}Ga_{0.81}N$ buffer. Notably in this context, we estimate that the different strain state of the two QWs only has a marginal influence on the band-gap energy and thus on the emission energy of the QWs. We estimated its influence on the emission energy by calculating the change of the bulk band-gap energy of an $In_{0.25}Ga_{0.75}N$ alloy, coherently grown on an $In_{0.19}Ga_{0.81}N$ buffer with varying degrees of plastic relaxation. For these calculations, we use simple continuum theory with the elastic- and lattice parameters from Ref. [29] and the deformation potentials from Ref. [30]. According to these calculations, a 30% partially relaxed $In_{0.19}Ga_{0.81}N$ buffer decreases the band gap of a coherently grown $In_{0.25}Ga_{0.75}N$ (bulk) layer by about 20 meV—which is negligible compared to the changes we observe in our PL experiments. Still, conclusions on the absolute concentrations only based on PL experiments are difficult due to a change of the charge-carrier localization within the QW. Details about these issues and its influence on the emission of comparable single monolayer thick QWs can be found elsewhere [28].

Summarizing our experimental data, we find a huge impact of strain on the incorporation of In into (0001) GaN: Growth on partially relaxed $In_{0.19}Ga_{0.81}N$ buffer (resulting in 0.6% tensile-strained GaN barriers) allows us to incorporate a more than two times higher In content. To gather an understanding of the underlying physical processes, we have calculated the

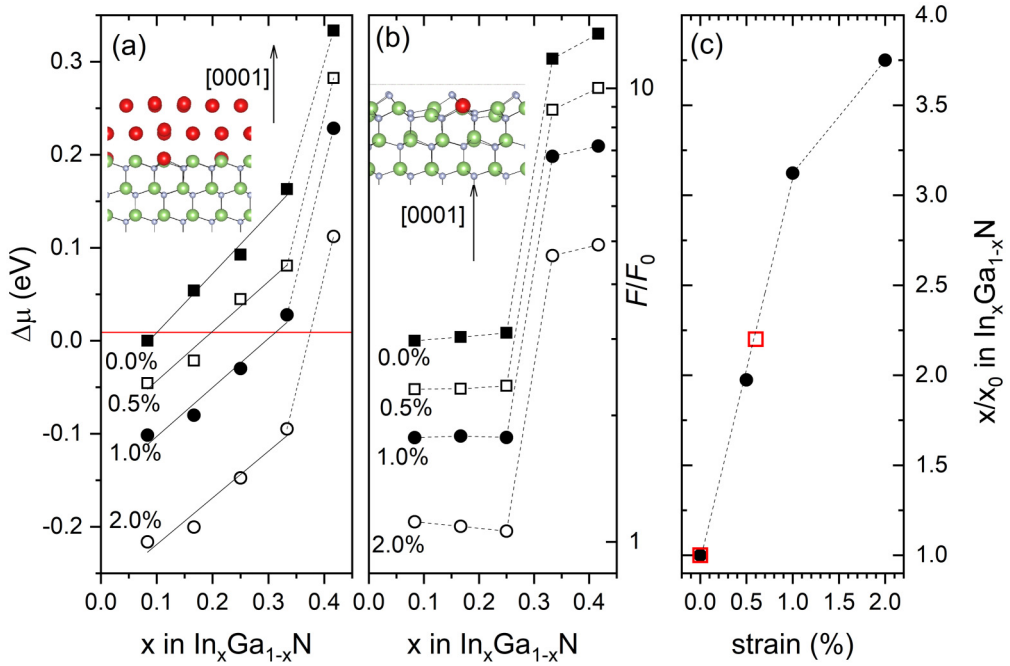

FIG. 6. (a), (b) Composition x in $In_xGa_{1-x}N$ as function of the chemical potential $\Delta\mu = \mu_{In} - \mu_{Ga}$ and the equivalent change in In fluxes [see Eq. (1)] at $T = 1229$ K as function of x for different basal plane tensile strains for metal-rich (a) and N-rich (b) growth conditions. The chemical potential to incorporate 1/12 In content at the GaN substrate (0.0% biaxial strain) is used as reference. F_0 is the reference flux at $\Delta\mu = -0.2163$ eV, i.e., the chemical potential required to incorporate 1/12 In content at 2% tensile strain under metal rich conditions. The horizontal red line indicates the experimentally relevant metal-rich conditions. The solid black lines in (a) are linear fits in the composition region $x = 1/12$ to $x = 4/12$. The dashed lines in (a) and (b) are guides to the eye. Insets: Ball and stick models in side view of the strain-free (0001) $In_{1/12}Ga_{11/12}N$ covered with an In bilayer (left) and the 2×2 N-adatom reconstruction (right). Large red and green balls indicate In and Ga atoms, respectively. Small gray balls are N atoms. (c) Calculated ratio $x/x0$ of the In content as a function of the substrate's biaxial strain state for metal-rich conditions [derived from (a)]. The values are referenced to the $In_xGa_{1-x}N$ composition of $x_0 = 0.1$ as realized on a GaN substrate (filled circles). Open rectangles correspond to experimental data.

change of the chemical potential $\Delta\mu = \mu_{In} - \mu_{Ga}$ associated with the exchange of a Ga by an In atom at the topmost III-N layer by DFT calculation. Thereby, we consider relaxed, as well as biaxially tensile-strained, GaN by 0.5, 1.0, and 2.0%, resembling growth on GaN and $In_xGa_{1-x}N$ buffers. We then successively replace Ga by In atoms at the energetically most favorable sites in the topmost III-N layer and compute the energy for a single substitution. The changes of the chemical potentials $\Delta\mu$ as a function of the In content for different strain states are plotted in Figs. 6(a) and 6(b) assuming metal- and N-rich growth conditions, respectively. Noticeably, the curve profiles for the two conditions behave quite differently. As it is discussed in detail in the following, this difference stems from the particular surfaces consisting of (i) an In bilayer for metal-rich and (ii) a N-adatom structure for N-rich conditions.

Let us first focus on the metal-rich case, as it is relevant for the growth experiments conducted in this work: For this calculation, we assume the presence of an In bilayer above the topmost III-N layer, as it is relevant for this case [31] [see inset in Fig. 6(a)]. In this context, it is worth mentioning that in our case the stability of the In bilayer depends on both the temperature and In flux [10] but not on the In incorporation into the GaN (0001) surface. Depletion of In from the bilayer will reduce the chemical potential of In at the surface, thus resulting in its refurbishment due to reestablishment of equilibrium conditions by a lower desorption rate of In atoms. For an In content ranging from 8 to 33%, In atoms are successively aligned as second-nearest neighbors in the metal sublattice of the topmost III-N layer, which ultimately leads to a $\sqrt{3} \times \sqrt{3}$ R30° configuration. Within this compositional range the chemical potential increases almost linearly by more than 100 meV. The primary reason for this is related to the presence of the metal bilayer: Incorporated In atoms in the topmost III-N layer are releasing strain via an outward relaxation causing a deformation of the metal bilayer thus increasing the surface tension. Exceeding In compositions of 33% results in a deviation from the linear relationship owing to an increased slope of the curve. This is caused by the necessity of In atoms now occupying first-nearest-neighbor sites in the metal sublattice, causing a considerable In-In strain repulsion [32]. For the sake of comparability, we have additionally considered a N-rich scenario, with the topmost GaN surface having a 2×2 N adatom reconstruction [see inset in Fig. 6(b)], as it is the energetically most favorable reconstruction under these conditions [33]. Here, the cations may occupy three- as well as fourfold bond configurations. For compositions up to 25%, In preferentially substitutes fourfold-coordinated Ga sites as second-nearest neighbors within the topmost III-N layer, as a consequence of the elastically frustrated rehybridization mechanism (see Ref. [23] for a detailed discussion). This

corresponds to a $2\sqrt{3} \times 2\sqrt{3}$ R30° surface configuration. Unlike the metal-rich scenario, in this case the change of the chemical potential is almost negligible [34], which is a consequence of the now possible free outward relaxation of the incorporated In atoms. Due to the aforementioned elastically frustrated rehybridization mechanism, In compositions above 25% immediately require substitution of Ga by In at first-nearest-neighbor sites. This results in a steep increase of the chemical potential by about 300 meV due to the repulsive In-In strain interactions. Regarding tensile-strained GaN, both considered growth scenarios show a strongly decreasing chemical potential of the incorporated In at the topmost III-N layer by about 100 meV per percent of tensile strain. In order to provide a more intuitive picture of the influence of tensile strain on the In incorporation for the samples investigated in this study, we employ statistical thermodynamics implementing the ideal gas model to map the changes in the chemical potential $\Delta\mu = \mu - \mu_o$ to changes into beam equivalent fluxes:

$$\Delta\mu = 2k_B T \ln(F/F_o), \tag{1}$$

where k_B and T, F, and F_o are the Boltzmann constant, the temperature of the effusion cell, the fluxes at μ and at a reference chemical potential μ_o, respectively. In our growth experiments, the In effusion cell temperature was set to $T = 1229$ K, which allows us to extend the diagrams for the metal- and N-rich case in Figs. 6(a) and 6(b) by a second ordinate, respectively. For metal-rich growth, as it is relevant for our growth experiments, increasing the In content from 10 to 33% requires an increased In flux by a factor of 2, as can be deduced from Fig. 6(a). Taking into account that our metal-rich MBE growth of $In_xGa_{1-x}N$ took place just before the onset of metal droplet formation to take advantage of the self-surfactant effect [31], such an increase will drive the system to a regime where $In_xGa_{1-x}N$ is unstable against bulk In, thus forming In droplets. Therefore, increasing the In flux under elsewise identical conditions will not result in a higher In content than the realized 10% in the QW on the GaN substrate. Nevertheless, this can be achieved by growth on an $In_xGa_{1-x}N$ buffer. For the present case, the increasing In content with tensile strain is indicated by the red horizontal line in Fig. 6(a). Following this line, growth conditions resulting in an In content of $\approx 10.0\%$ on an unstrained GaN substrate, would increase the In content to approximately 20, 31, and 37% on GaN with tensile strains of 0.5, 1, and 2%, respectively, as it is plotted in Fig. 6(c). Hence, starting from an In content of 10% on GaN, we would expect an increase of the In content to about 22% for growth on our $In_{0.19}Ga_{0.81}N$ buffers (corresponding to 0.6% of tensile strain). This is in very good agreement with our experimental data [see red rectangles in Fig. 6(c)]. Hence, with regard to metal-rich growth, increased In incorporation at a given In flux is achieved owing to the decrease of the chemical potential with tensile strain. For compositions above 33%, the slope the curve in Fig. 6(c) decreases due to the repulsive strain interaction of In atoms now occupying first-nearest-neighbor sites in the metal sublattice. This strain interaction represents a considerable barrier.

Turning to N-rich MBE conditions, the increase of the chemical potential with In content is mainly governed by the fourfold coordination of In in the 2×2 N adatom structure. While this immediately allows us to achieve In composition up to 25% a huge energy barrier of 300 meV is necessary to overcome when exceeding this value. As for the metal-rich case, this is again due to the In-In repulsion now necessarily occupying next-nearest-neighbor sites. Thus, growth on an $In_{0.19}Ga_{0.81}N$ will not directly result in an increased In incorporation during growth. Instead, in this case tensile strain is effective by reducing thermal decomposition due to the stabilization of the In–N bond.

IV. CONCLUSIONS

In summary, we have analyzed the In incorporation in tensile-strained GaN surfaces considering metal- as well as N-rich growth conditions at the atomic level. For both growth scenarios, we observe a strongly decreasing chemical potential of the system with increasing tensile strain of the GaN. This is independent on the particular surface reconstruction and thus accounts for a variety of different growth conditions. The gain with respect to achieve higher In compositions can be twofold: Incorporation of In is directly promoted at a given In flux (metal rich) and/or thermal decomposition is reduced via stabilization of the In–N bond (N rich). Our calculations are quantitatively confirmed by MBE growth experiments showing a more than two times higher In content in a QW grown on a partially relaxed $In_{0.19}Ga_{0.81}N$ as compared to growth on GaN. Although we find that metal-rich MBE conditions to be more beneficial for achieving higher In compositions by reducing the strain, experimental data for metal organic vapor phase epitaxy (MOVPE) growth reveal comparable effects, despite it is generally considered as being intrinsically N rich [16–19,35]. For instance, a 3× higher In incorporation is observed at islands and plastically relaxed layers in Refs. [16,17]. Despite that in these experiments it is much more difficult to assess the strain state of the layer due to a transition of the growth mode, our results may still qualitatively explain the observed effect. Though the energetically favorable surface reconstructions are different in MOVPE [36], the stabilization of the In–N bond against thermal decomposition should be of comparable magnitude thus increasing In content in the layer. Hence, despite the In-In strain interaction on first-nearest-neighbor sites posing in the same manner a considerable obstacle for achieving In contents above 33%, strain engineering via growth on $In_xGa_{1-x}N$ buffers provides routes to increase the composition of $In_xGa_{1-x}N$ QWs in MBE as well as MOVPE.

ACKNOWLEDGMENTS

This work has been partially supported by the European Union within SPRInG Grant No. 642574. We thank E. Grzanka for x-ray diffraction and G. Staszczak for photoluminescence measurements.

[1] T. Mehrtens, M. Schowalter, D. Tytko, P. Choi, D. Raabe, L. Hoffmann, H. Jönen, U. Rossow, A. Hangleiter, and A. Rosenauer, Appl. Phys. Lett. **102**, 132112 (2013).

[2] T. Suski, T. Schulz, M. Albrecht, X. Q. Wang, I. Gorczyca, K. Skrobas, N. E. Christensen, and A. Svane, Appl. Phys. Lett. **104**, 182103 (2014).

[3] A. Yoshikawa, S. B. Che, W. Yamaguchi, H. Saito, X. Q. Wang, Y. Ishitani, and E. S. Hwang, Appl. Phys. Lett. **90**, 073101 (2007).

[4] R. Averbeck and H. Riechert, Phys. Status Solidi A **176**, 301 (1999).

[5] N. Yoshimoto, T. Matsuoka, T. Sasaki, and A. Katsui, Appl. Phys. Lett. **59**, 2251 (1991).

[6] I. H. Ho and G. B. Stringfellow, Appl. Phys. Lett. **69**, 2701 (1996).

[7] C. K. Gan, Y. P. Feng, and D. J. Srolovitz, Phys. Rev. B **73**, 235214 (2006).

[8] S. Y. Karpov, MRS Internet J. Nitride Semicond. Res. **3**, e16 (1998).

[9] A. Tabata, L. K. Teles, L. M. R. Scolfaro, J. R. Leite, A. Kharchenko, T. Frey, D. J. As, D. Schikora, K. Lischka, J. Furthmüller, and F. Bechstedt, Appl. Phys. Lett. **80**, 769 (2002).

[10] A. I. Duff, L. Lymperakis, and J. Neugebauer, Phys. Status Solidi B **252**, 855 (2015).

[11] A. I. Duff, L. Lymperakis, and J. Neugebauer, Phys. Rev. B **89**, 085307 (2014).

[12] Y. Inatomi, Y. Kangawa, T. Ito, T. Suski, Y. Kumagai, K. Kakimoto, and A. Koukitu, Jpn. J. Appl. Phys. **56**, 078003 (2017).

[13] K. Hiramatsu, Y. Kawaguchi, M. Shimizu, N. Sawaki, T. Zheleva, R. F. Davis, H. Tsuda, W. Taki, N. Kuwano, and K. Oki, MRS Internet J. Nitride Semicond. Res. **2**, U3 (1997).

[14] Y. Kawaguchi, M. Shimizu, K. Hiramatsu, and N. Sawaki, MRS Proc. **449**, 89 (1996).

[15] S. Pereira, M. R. Correia, E. Pereira, K. P. O'Donnell, C. Trager-Cowan, F. Sweeney, and E. Alves, Phys. Rev. B **64**, 205311 (2001).

[16] M. Pristovsek, J. Stellmach, M. Leyer, and M. Kneissl, Phys. Status Solidi C **6**, S565 (2009).

[17] M.-I. Richard, M. J. Highland, T. T. Fister, A. Munkholm, J. Mei, S. K. Streiffer, C. Thompson, P. H. Fuoss, and G. B. Stephenson, Appl. Phys. Lett. **96**, 051911 (2010).

[18] A. Even, G. Laval, O. Ledoux, P. Ferret, D. Sotta, E. Guiot, F. Levy, I. C. Robin, and A. Dussaigne, Appl. Phys. Lett. **110**, 262103 (2017).

[19] S. S. Pasayat, C. Gupta, D. Acker-James, D. A. Cohen, S. P. DenBaars, S. Nakamura, S. Keller, and U. K. Mishra, Semicond. Sci. Technol. **34**, 115020 (2019).

[20] L. Lymperakis, T. Schulz, C. Freysoldt, M. Anikeeva, Z. Chen, X. Zheng, B. Shen, C. Chèze, M. Siekacz, X. Q. Wang, M. Albrecht, and J. Neugebauer, Phys. Rev. Mater. **2**, 011601 (2018).

[21] See Supplemental Material at http://link.aps.org/supplemental/10.1103/PhysRevMaterials.4.073404 for a reciprocal space map, scanning transmission electron microscopy high angle annular dark field images simulations and transmission electron microcopy images.

[22] J. Moneta, M. Siekacz, E. Grzanka, T. Schulz, T. Markurt, M. Albrecht, and J. Smalc-Koziorowska, Appl. Phys. Lett. **113**, 031904 (2018).

[23] T. Schulz, T. Remmele, T. Markurt, M. Korytov, and M. Albrecht, J. Appl. Phys. **112**, 033106 (2012).

[24] E. C. Do, Y.-H. Shin, and B.-J. Lee, J. Phys.: Condens. Matter **21**, 325801 (2009).

[25] A. Chuvilin and U. Kaiser, Ultramicroscopy **104**, 73 (2005).

[26] P. A. Stadelmann, Ultramicroscopy **21**, 131 (1987).

[27] E. J. Kirkland, R. F. Loane, and J. Silcox, Ultramicroscopy **23**, 77 (1987).

[28] M. Anikeeva, M. Albrecht, F. Mahler, J. W. Tomm, L. Lymperakis, C. Chèze, R. Calarco, J. Neugebauer, and T. Schulz, Sci. Rep. **9**, 9047 (2019).

[29] A. F. Wright, J. Appl. Phys. **82**, 2833 (1997).

[30] Q. Yan, P. Rinke, A. Janotti, M. Scheffler, and C. G. Van de Walle, Phys. Rev. B **90**, 125118 (2014).

[31] J. Neugebauer, T. K. Zywietz, M. Scheffler, J. E. Northrup, H. Chen, and R. M. Feenstra, Phys. Rev. Lett. **90**, 056101 (2003).

[32] S. Lee, C. Freysoldt, and J. Neugebauer, Phys. Rev. B **90**, 245301 (2014).

[33] J. E. Northrup, J. Neugebauer, R. M. Feenstra, and A. R. Smith, Phys. Rev. B **61**, 9932 (2000).

[34] In fact, the gradient of the chemical potential with respect to the composition x has finite values, although very small. This is more evident for the case of 2% tensile strain where the slope becomes negative. At 2% biaxial tensile strain, the basal plane lattice constant of the GaN host matrix is approximately equal to that of a fully relaxed InGaN alloys with ≈18% In content. Therefore, In incorporation allows for a reduction of the tensile strain built in the host matrix and hence results in the negative slope of the chemical potential.

[35] G. Ju, M. Tabuchi, Y. Takeda, and H. Amano, Appl. Phys. Lett. **110**, 262105 (2017).

[36] C. G. Van de Walle and J. Neugebauer, Phys. Rev. Lett. **88**, 066103 (2002).